Nanoscale Metal–Organic Framework Overcomes Hypoxia for Photodynamic Therapy Primed Cancer Immunotherapy

Guangxu Lan[†,‡], **Kaiyuan Ni**[†,‡], **Ziwan Xu**[†,⊥], **Samuel S. Veroneau**[†], **Yang Song**[†], and **Wenbin Lin**[†,§,*]

[†]Department of Chemistry, The University of Chicago, Chicago, Illinois 60637, United States

[§]Department of Radiation and Cellular Oncology and Ludwig Center for Metastasis Research, The University of Chicago, Chicago, Illinois 60637, United States

[⊥]College of Chemistry and Molecular Engineering, Peking University, Beijing 100871, China

Abstract

Immunotherapy has become a promising cancer therapy, but only works for a subset of cancer patients. Immunogenic photodynamic therapy (PDT) can prime cancer immunotherapy to increase the response rates, but its efficacy is severely limited by tumor hypoxia. Here we report a nanoscale metal–organic framework, Fe-TBP, as a novel nanophotosensitizer to overcome tumor hypoxia and sensitize effective PDT, priming non-inflamed tumors for cancer immunotherapy. Fe-TBP was built from iron-oxo clusters and porphyrin ligands and sensitized PDT under both normoxic and hypoxic conditions. Fe-TBP mediated PDT significantly improved the efficacy of anti-programmed death-ligand 1 (α-PD-L1) treatment and elicited abscopal effects in a mouse model of colorectal cancer, resulting in >90% regression of tumors. Mechanistic studies revealed that Fe-TBP mediated PDT induced significant tumor infiltration of cytotoxic T cells.

Cancer immunotherapy has recently emerged as a highly effective cancer treatment.[1] Immune checkpoint blockade (ICB), which uses antibodies to block negative immune regulatory pathways,[2] has enjoyed clinical success for several advanced cancers.[3] However, due to insufficient activation of host immune systems, ICB elicits limited rates of systemic antitumor responses for many cancers.[4] Combining ICB with other immunogenic treatments may increase response rates of non-inflamed tumors.[5] Photodynamic therapy (PDT) causes acute inflammatory responses to alter the tumor microenviron-ment,[6] promising to

[*]Corresponding Author: wenbinlin@uchicago.edu.
[‡]**Author Contributions**
These authors contributed equally.
ORCID
Guangxu Lan: 0000-0002-0415-5849
Kaiyuan Ni: 0000-0002-8152-6746
Ziwan Xu: 0000-0001-9459-4572
Wenbin Lin: 0000-0001-7035-7759

significantly enhance ICB efficacy. Synergistic combination of PDT and ICB, however, is rarely explored.[7]

A new class of nanophotosensitizers (nPSs) based on nanoscale metal–organic frameworks (nMOFs)[8] have recently emerged as highly effective photosensitizers (PSs) for PDT. nMOF-based nPSs directly incorporate PSs as the building units, allowing for high PS loadings without self-quenching.[9] The porous structures of nMOFs also facilitate the diffusion of reactive oxygen species (ROS), improving the PDT efficacy of nMOFs over other nPSs. However, the efficacy of nPS-mediated PDT is still limited by tumor hypoxia. Herein we report the design of a novel nMOF-based nPS, Fe-TBP, to overcome hypoxia and enhance cancer immunotherapy. Fe-TBP was constructed from Fe_3O clusters and 5,10,15,20-tetra(p-benzoato)porphyrin (TBP) ligand, and, when irradiated under hypoxic conditions, catalyzed a cascade reaction in which intracellular H_2O_2 was decomposed by the Fe_3O clusters to produce O_2 through a Fenton-like reaction whereas the generated O_2 was converted to cytotoxic singlet oxygen ($^1O_2$) by photoexcited porphyrins (Figure S1a, SI). Fe-TBP mediated PDT elicited systemic antitumor response to improve the α-PD-L1 ICB, leading to the regression of both treated primary tumors and untreated distant tumors via abscopal effects (Figure 1a).

Fe-TBP was synthesized from $[Fe_3O(OAc)_6(H_2O)_3]OAc$ (OAc = acetate) and H_4TBP solvothermally (Figure S1b, SI) and showed a nanorice morphology (Figure 1b). The crystallinity of Fe-TBP was confirmed by the lattice structure and fast Fourier transform (FFT) pattern in TEM images (Figure 1c). By tuning reagent concentrations (Figure S2, S3, SI), we optimized the Fe-TBP nanorice to 100 nm in length (Figure 1d), an ideal size for nanocarriers.[10] This 100 nm Fe-TBP showed effective cellular uptake (Figure S4, SI) and was used in subsequent studies. Powder X-ray diffraction (PXRD) studies indicated that Fe-TBP adopted the PCN-600 structure (Figure 1e).[11] Fe-TBP showed type I nitrogen sorption isotherms at 77 K (Figure S5, SI) with a Brunauer–Emmett–Teller (BET) surface area of 526.0 m^2/g. The UV–vis spectra indicated the presence of the TBP ligands (Figure 1f) whereas extended X-ray absorption fine structure (EXAFS) analysis verified the $Fe_3O(carboxylate)_6(H_2O)_3^+$ coordination environment in Fe-TBP (Figure 1f and Table S1, SI). The Fe^{3+} centers were confirmed by X-ray absorption near edge spectroscopy (Figure S6a, SI). The Fe to TBP ratio was determined to be 2.13 or 2.21 by inductively coupled plasma-mass spectrometry (ICP-MS) or thermogravimetric analysis (Figure S6b, SI), respectively. The slightly higher Fe to TBP ratio is due to the nanosize of and possibly defects in Fe-TBP.

Because hypoxic cancer cells usually have high H_2O_2 concentrations, converting intracellular H_2O_2 into O_2 through a Fenton reaction is an effective way to overcome hypoxia.[12] We conducted several studies to determine the ability of Fe- TBP in catalyzing the decomposition of H_2O_2 to generate O_2. First, H_2O_2 at an intracellular concentration of 100 μM with or without Fe-TBP was added to an oxygen-free phosphate buffer solution (PBS) at 37 °C. The time-dependent O_2 concentration was then detected by an oxygen sensor to reveal the production of a significant amount of O_2 by Fe-TBP (Figure 2a). To demonstrate the catalytic effect of Fe-TBP at the cellular level, the intracellular H_2O_2 concentration was assessed using a fluorescent peroxide assay kit. Under hypoxic

conditions, strong green fluorescence was observed, indicating a high H_2O_2 level. The fluorescence intensity decreased dramatically after treatment with Fe-TBP, confirming that Fe-TBP decomposed intracellular H_2O_2, while no fluorescence decrease was observed in the H_4TBP control group (Figure 2d). This catalytic effect of Fe-TBP was also demonstrated by adding Fe-TBP to H_2O_2 pretreated cells under normoxic condition (Figure S7, SI). The stability of Fe-TBP in PBS and during Fenton reaction was demonstrated by PXRD (Figure S8, SI). We further proved the ability of Fe-TBP in reducing hypoxia by evaluating the expression of hypoxia-inducible factor 1-α (HIF-1α) protein, which is typically upregulated under hypoxic condition. Incubation of cells under low oxygen conditions induced the accumulation of HIF-1α. When treated with Fe-TBP, a significant reduction in HIF-1α fluorescence intensity was observed (Figure 2e). Immunohistochemistry staining of HIF-1α further confirmed that Fe-TBP highly alleviated hypoxia in tumor tissues (Figure 2f). These data demonstrate that Fe-TBP can effectively overcome hypoxia at cellular to tumor levels.

We next determined whether Fe-TBP could effectively mediate PDT under hypoxic condition. Hf-TBP, an nMOF constructed from Hf-based clusters and TBP ligands with similar size and morphology, was used as a control (Figure S9, SI). First, the $^1O_2$ generation efficacy of Fe-TBP was determined by the Singlet Oxygen Sensor Green (SOSG). Fe-TBP effectively generated $^1O_2$ in irradiation-dependent manner in PBS under normoxic condition (Figure 2b). In oxygen-free solutions, Fe-TBP showed almost no $^1O_2$ generation upon irradiation. However, upon the addition of H_2O_2 to oxygen-free PBS or DMF, Fe-TBP showed similar $^1O_2$ generation to the normoxic condition (Figure 2c, S10, and S11, SI). In contrast, upon irradiation, both H_4TBP and Hf-TBP generated only trace amounts of $^1O_2$ in oxygen-free, H_2O_2-containing PBS. Under normoxic condition, Hf-TBP and H_4TBP showed inferior PDT efficacy to Fe-TBP with IC_{50} values of 2.60 ± 1.59, 11.33 ± 6.75, and 25.13 ± 6.83 μM for Fe-TBP, Hf-TBP, and H_4TBP, respectively (Figure 2g and S12, SI). Under hypoxic condition, Fe-TBP exhibited comparable PDT efficacy with an IC_{50} of 3.10 ± 1.66 μM while Hf-TBP and H_4TBP were totally ineffective with IC_{50} values much greater than 50 μM (Figure 2h). To confirm the superb PDT efficacy of Fe-TBP in tumors, we employed a mouse model of CT26 colorectal adenocarcinoma due to its typically hypoxic nature.[13] After PDT treatment, Fe-TBP effectively regressed locally irradiated tumors, while Hf-TBP and H_4TBP treated groups showed only moderate anticancer efficacy (Figure 2i and S13a,b, SI). No dark toxicity of Fe-TBP was observed (Figure S13g, SI) and ICP-MS analysis showed that Fe-TBP mostly remained in tumors 4 h after incubation and was cleared in 10 days (Figure S14, SI). Our data confirm that Fe-TBP mediates effective PDT under both normoxic and hypoxic conditions.

We next investigated whether Fe-TBP mediated PDT could improve cancer immunotherapy. First, we studied the cell death pathway of Fe-TBP mediated PDT to evaluate whether Fe-TBP can activate the host immune system. After PDT treatment, significant amounts of Fe-TBP treated cells underwent apoptosis/necrosis with only 18.8% of cells remaining healthy (Figure S15 and S16, SI) and obvious morphological changes with decreasing cell intensity were observed (Figure S17). The immunogenic cell death (ICD) induced by PDT treatment was investigated by detecting cell-surface exposure of calreticulin (CRT). Strong green fluorescence of CRT was observed in Fe-TBP treated cells and quantified by flow cytometry

(Figure S18 and S19, SI). Immunostaining analysis confirmed high CRT expression in Fe-TBP treated tumors (Figure 3a).

We then tested the anticancer effect on a bilateral model of CT26 tumors on BALB/c mice. One of the tumors (primary) was treated with Fe-TBP and irradiated, while the other tumor (distant) was untreated. The mice then underwent a-PD-L1 treatment. The mice treated with light only, Fe-TBP plus light, or a-PD-L1 plus light served as controls. The immunotherapeutic efficacy of different treatment regimens was assessed by the growth rates of both the primary and distant tumors. We found that Fe-TBP mediated PDT significantly improved the a-PD-L1 treatment by eliciting consistent abscopal effects, leading to >90% regression of both tumors at a low Fe-TBP dose of 0.2 μmol based on TBP and light dose of 45 J/cm^2 (Figure 3b,c, and S13c–f, SI). Fe-TBP plus a-PD-L1 group showed necrotic tumor histology in the untreated distant tumor (Figure S20, SI). In contrast, only a slight abscopal effect was observed in the mice treated with Fe-TBP and no abscopal effect was observed for mice treated with a-PD-L1 (Figure 3c). The body weights of mice remained consistent, regardless of treatment, suggesting no systemic toxicity (Figure S13h, SI). To confirm the long-term antitumor immune response, we carried out a tumor challenge study, wherein the cured mice successfully rejected tumor challenge (injection of 2×10^6 CT26 cells) 30 days post-tumor eradication (Figure 3e). Our results demonstrate that Fe-TBP mediated PDT improves the ICB efficacy and promotes abscopal effects.

We next determined the mechanism by which Fe-TBP-mediated PDT enhanced the ICB efficacy. We first found that Fe-TBP plus a-PD-L1 treatment lost the immunotherapeutic efficacy after depletion of either B cells or CD4$^+$ or CD8$^+$ T cells on single tumor model, indicating the involvement of these cells (Figure 3d). We then tested the antitumor immunity of CT26-bearing mice treated with Fe-TBP plus a-PD-L1 by Enzyme-Linked ImmunoSpot (ELISPOT) and immune cell profiling. We determined the presence of tumor-antigen specific cytotoxic T cells with an IFN-γ ELISPOT assay. At day 10 after the PDT treatment, splenocytes were harvested from CT26-bearing mice and stimulated with SPSYVYHQF, a tumor associated antigen, for 42 h and the IFN-γ spot forming cells were counted. The number of antigen-specific IFN-γ producing T cells significantly increased in tumor-bearing mice treated with Fe-TBP plus a-PD-L1 (96.9 ± 20.9 compared to 16.3 ± 4.1 for PBS or 63.9 ± 36.7 for Fe-TBP, Figure 4a), suggesting that Fe-TBP plus a-PD-L1 treatment induced tumor-specific T cell response. We further profiled infiltrating leukocytes in tumors (Figure S21). The Fe-TBP plus a-PD-L1 group showed significant increase of tumor-infiltrating CD4$^+$ and CD8$^+$ T cells in both primary and distant tumors (Figure 4c,d). The infiltration of CD8$^+$ T cells was further confirmed by immunostaining (Figure S22, SI). The Fe-TBP with or without antibody treated groups showed significant increase of tumor-infiltrating CD45$^+$ T cells and B cells in the primary tumors (Figure 4b, S23a, SI). Interestingly, the distant tumors of Fe-TBP plus a-PD-L1 treated group showed significant increase of dendritic cells (Figure S23b, SI). Also, we found significant decrease of monocytes in the primary tumors in Fe-TBP with or without a-PD-L1 groups (Figure S23c, SI). In addition, regulatory T cells significantly decreased in lymph nodes (Figure S24b, SI). Taken together, Fe-TBP-mediated PDT plus a-PD-L1 treatment alleviates the immunosuppression and increases the infiltration of effector T cells.

In summary, we have developed a novel nMOF to overcome tumor hypoxia in PDT and improve cancer immunotherapy. Fe-TBP plus a-PD-L1 treatment induces significant expansions of both CD4^{+} and CD8^{+} cytotoxic T cells, which infiltrate distant tumors to elicit abscopal effects. Our study presents a novel strategy to combining PDT with ICB to elicit systemic antitumor immunity.

Supplementary Material

Refer to Web version on PubMed Central for supplementary material.

Acknowledgments

References

1. (a)McNutt M. Science. 2013; 342(6165):1417. [PubMed: 24357273] (b)Luo M, Wang H, Wang Z, Cai H, Lu Z, Li Y, Du M, Huang G, Wang C, Chen X, Porembka M, Lea J, Frankel A, Fu Y, Chen Z, Gao J. Nat Nanotechnol. 2017; 12:648–654. [PubMed: 28436963]

2. Pardoll DM. Nat Rev Cancer. 2012; 12(4):252–264. [PubMed: 22437870]

3. (a)Brahmer JR, Tykodi SS, Chow LQ, Hwu WJ, Topalian SL, Hwu P, Drake CG, Camacho LH, Kauh J, Odunsi K. New Engl J Med. 2012; 366:2455–2465. [PubMed: 22658128] (b)Topalian SL, Hodi FS, Brahmer JR, Gettinger SN, Smith DC, McDermott DF, Powderly JD, Carvajal RD, Sosman JA, Atkins MB. New Engl J Med. 2012; 366:2443–2454. [PubMed: 22658127]

4. Sharma P, Allison JP. Science. 2015; 348(6230):56–61. [PubMed: 25838373]

5. Min Y, Roche KC, Tian S, Eblan MJ, McKinnon KP, Caster JM, Chai S, Herring LE, Zhang L, Zhang T, et al. Nat Nanotechnol. 2017; 12(9):877. [PubMed: 28650437]

6. (a)Spring BQ, Sears RB, Zheng LZ, Mai Z, Watanabe R, Sherwood ME, Schoenfeld DA, Pogue BW, Pereira SP, Villa E, et al. Nat Nanotechnol. 2016; 11(4):378–387. [PubMed: 26780659] (b)Lovell JF, Jin CS, Huynh E, Jin H, Kim C, Rubinstein JL, Chan WC, Cao W, Wang LV, Zheng G. Nat Mater. 2011; 10(4):324–332. [PubMed: 21423187] (c)Huang P, Lin J, Wang X, Wang Z, Zhang C, He M, Wang K, Chen F, Li Z, Shen G, et al. Adv Mater. 2012; 24(37):5104–5110. [PubMed: 22718562] (d)Marrache S, Choi JH, Tundup S, Zaver D, Harn DA, Dhar S. Integr Biol. 2013; 5(1): 215–223.

7. (a)Lu K, He C, Guo N, Chan C, Ni K, Weichselbaum RR, Lin W. J Am Chem Soc. 2016; 138(38): 12502–12510. [PubMed: 27575718] (b)He C, Duan X, Guo N, Chan C, Poon C, Weichselbaum RR, Lin W. Nat Commun. 2016; 7:12499. [PubMed: 27530650]

8. (a)Lu K, He C, Lin W. J Am Chem Soc. 2014; 136(48):16712–16715. [PubMed: 25407895] (b)Fateeva A, Chater PA, Ireland CP, Tahir AA, Khimyak YZ, Wiper PV, Darwent JR, Rosseinsky MJ. Angew Chem. 2012; 124(30):7558–7562. (c)Xu H, Liu F, Cui Y, Chen B, Qian G. Chem Commun. 2011; 47(11):3153–3155. (d)Park J, Jiang Q, Feng D, Mao L, Zhou HC. J Am Chem Soc. 2016; 138(10):3518–3525. [PubMed: 26894555] (e)Furukawa H, Cordova KE, O'Keeffe M, Yaghi OM. Science. 2013; 341(6149):1230444. [PubMed: 23990564] (f)Levine DJ, Runčevski Te, Kapelewski MT, Keitz BK, Oktawiec J, Reed DA, Mason JA, Jiang HZ, Colwell KA, Legendre CM, et al. J Am Chem Soc. 2016; 138(32):10143–10150. [PubMed: 27486905] (g)Morris W, Briley WE, Auyeung E, Cabezas MD, Mirkin CA. J Am Chem Soc. 2014; 136(20):7261–7264. [PubMed: 24818877]

9. Lan G, Ni K, Lin W. Coord Chem Rev. 2017; doi: 10.1016/j.ccr.2017.09.007

10. Panyam J, Labhasetwar V. Adv Drug Delivery Rev. 2003; 55(3):329–347.

11. Wang K, Feng D, Liu TF, Su J, Yuan S, Chen YP, Bosch M, Zou X, Zhou HC. J Am Chem Soc. 2014; 136(40):13983–13986. [PubMed: 25208035]

12. Kim J, Cho HR, Jeon H, Kim D, Song C, Lee N, Choi SH, Hyeon T. J Am Chem Soc. 2017; 139(32):10992–10995. [PubMed: 28737393]

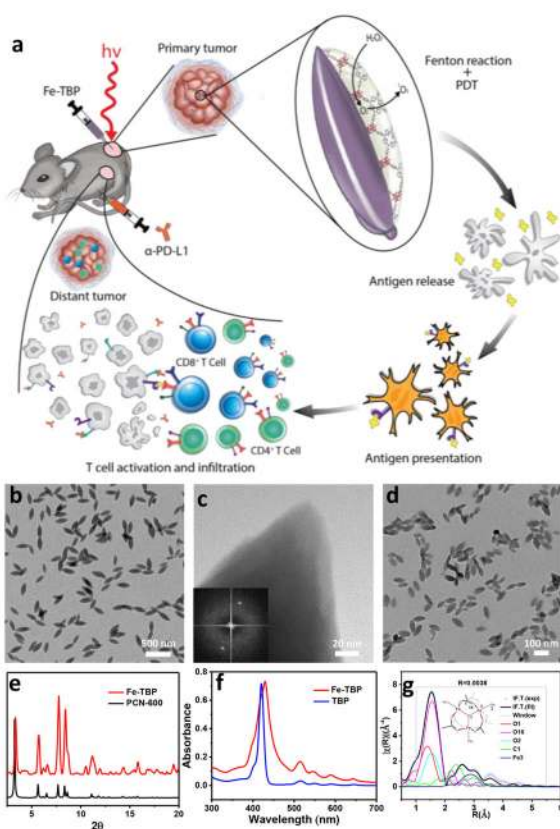13. Mizukami Y, Chung DC. Current Colorectal Cancer Reports. 2007; 3(2):71–75.

Figure 1.
(a) Schematic illustration of using Fe-TBP to overcome hypoxia for PDT primed cancer immunotherapy. (b) TEM image of Fe-TBP. (c) High-resolution TEM image and fast Fourier transform (inset) of Fe-TBP. (d) TEM image of optimized 100 nm Fe-TBP. (e) PXRD pattern of Fe-TBP in comparison to PCN-600. (f) UV–visible spectra of Fe-TBP and H_4TBP. (g) EXAFS fitting of Fe-TBP, showing the Fe coordination environment as $Fe_3O(carboxylate)_6(H_2O)_3^+$.
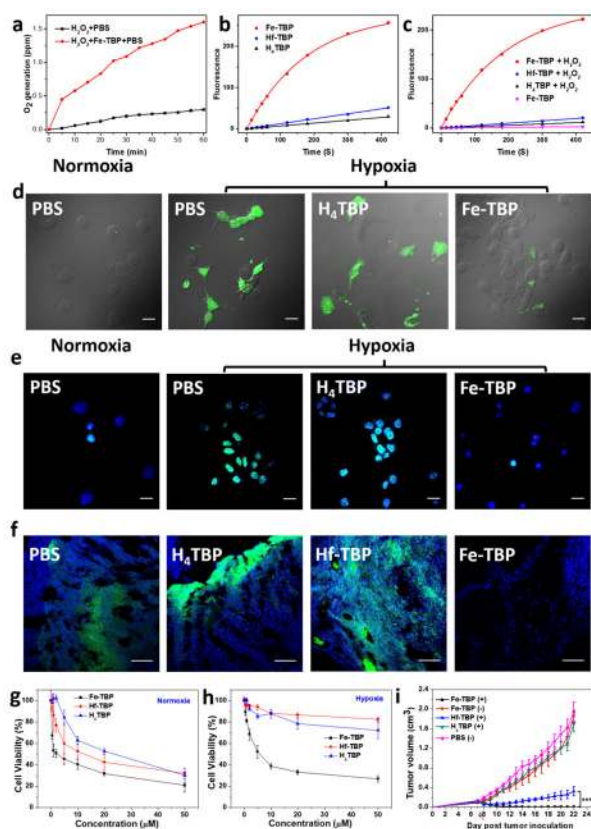
Figure 2.
Fe-TBP overcomes hypoxia by converting H_2O_2 into O_2. (a) Time-dependent O_2 generation detected by an oxygen sensor. $^1O_2$ generation under normoxic condition (b) and hypoxic condition (c) detected by SOSG assay. (d) CLSM images of green fluorescence detecting intracellular H_2O_2. Scale bar = 20 μm. (e) CLSM images of green fluorescent intranuclear HIF-1α expression in cells. Scale bar = 20 μm. (f) *In vivo* HIF-1α expression was evaluated on sectioned tumor slides of CT26-bearing mice. Scale bar = 100 μm. Cytotoxicity tests under normoxic condition (g) and hypoxic condition (h). (i) Tumor growth curves of CT26 tumor bearing mice treated with PBS, H_4TBP, Hf-TBP or Fe-TBP with light irradiation or Fe-TBP without light irradiation. $N = 6$.
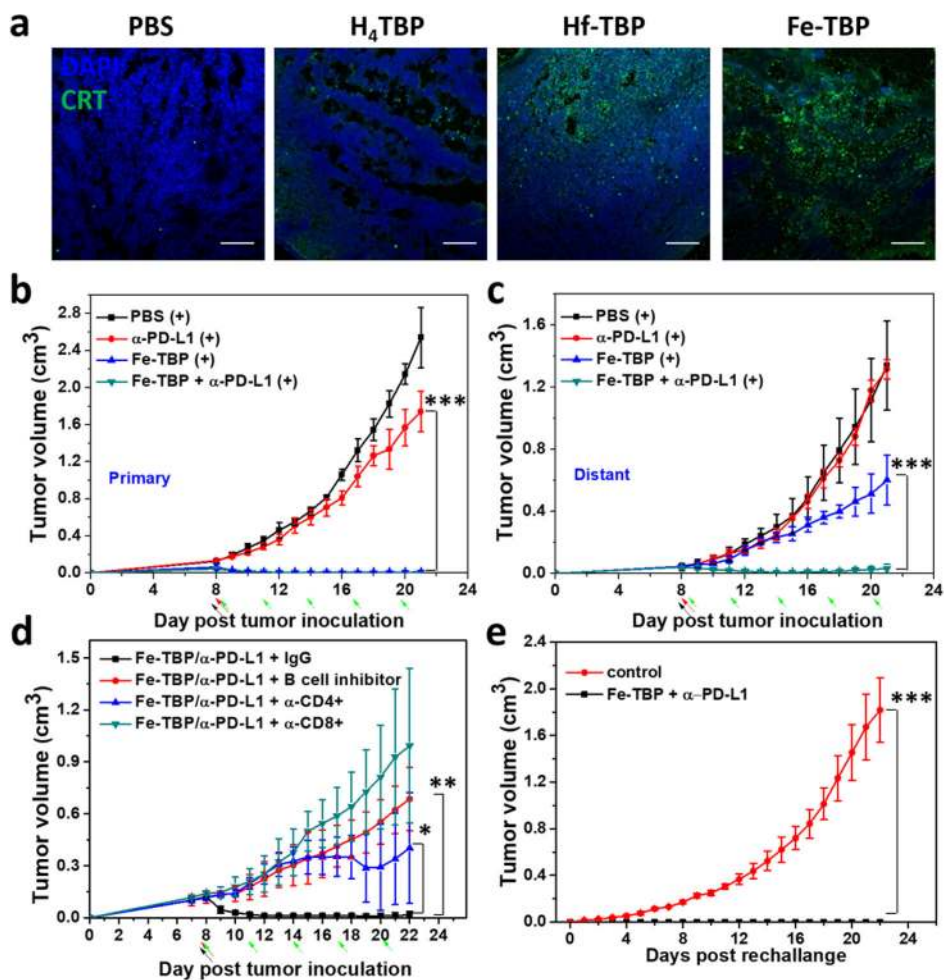
Figure 3.
Fe-TBP mediated PDT caused ICD and primed cancer immunotherapy. (a) *In vivo* immunofluorescence of CRT exposure shown by green fluorescence. Growth curves of primary tumors (b) and distant tumors (c) of bilateral CT26 tumor-bearing mice. $N = 6$. (d) Tumor growth curves of CT26 tumor bearing mice with T cell or B cell depletion. (e) Tumor growth curves after challenged with CT26 cells. $N = 6$. *$P < 0.05$, **$P < 0.01$, and ***$P < 0.001$.
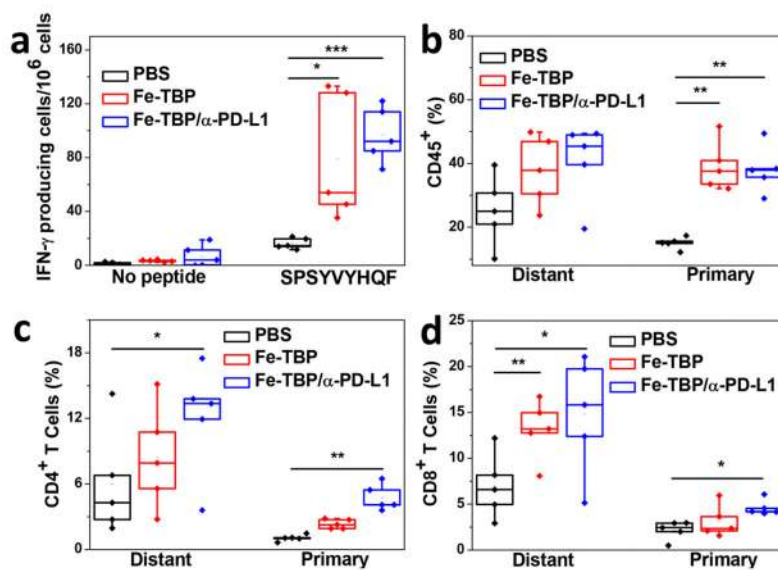
Figure 4.
Tumor-specific immune responses. (a) ELISPOT assay was performed to detect IFN-γ producing T cells. The percentage of tumor-infiltrating CD45$^+$ cells (b), CD4$^+$ T cells (c), and CD8$^+$ T cells (d) with respect to the total tumor of cells. Data are expressed as means ± s.d. (n = 5). *P < 0.05, **P < 0.01, and ***P < 0.001 from control.